Modeling the non-linearities of charge-transfers and solid electrolyte interphase resistances for a sodium-ion battery with a hard carbon electrode

Houssam Rabab, Nicolas Damay, Fernanda Vendrame, Christophe Forgez, Asmae El Mejdoubi

Modeling the non-linearities of charge-transfers and solid electrolyte interphase resistances for a sodium-ion battery with a hard carbon electrode

Houssam Rabab · Nicolas Damay · Fernanda Vendrame · Christophe Forgez · Asmae El Mejdoubi

Abstract Sodium-ion batteries are a promising technology whose performance are getting closer to those of lithium-ion batteries. The electrochemical phenomena are mostly the same for these two technologies, but the sodium-ion battery studied in this paper has a negative electrode made of hard carbon "HC" in which different phenomenon occurs when state of charge "SoC" decreases. In this paper, we characterized this sodium-ion battery thanks to a physic-based model that can represent the non-linearities of the charge transfers and solid electrolyte interphase "SEI" resistances. In this initial study, we found that this model represented accurately the battery non-linearities for high SoC, making it able to characterize its charge transfers and SEI (eg. for diagnosis purpose). However, the model failed to represent the cell behavior below SoC 40-50%, suggesting that it should be improved for batteries with HC electrodes.

1 Introduction

The need for various energy storage technologies is increasing significantly. Currently, lithium-ion batteries remain the most widely used. However, because of increasing demands of rechargeable batteries, and since lithium is not sufficiently abundant compared to the market needs, the search for alternatives is being motivated. These alternatives should be more efficient, less expensive and more sustainable, which is the case of sodium-ion batteries developped by Tiamat [1]. Therefore, we use Tiamat cell of $Na_3V_2(PO_4)_2F_3$/hard carbon type, denoted NVPF/HC, for this article.

Nicolas Damay
Laboratoire Roberval
Université de Technologie de Compiègne
Centre de Recherches Royallieu, CS 60319
60203 Compiègne Cedex, France
e-mail: nicolas.damay@utc.fr

NVPF/HC cells rely on hard carbon "HC" as a negative electrode instead of graphite, because the graphite offers limited electrochemical performance [2]. In fact, the size of sodium ion is larger than that of lithium ion [3], which causes insertion difficulties of Na^+ in the crystalline structure of graphite.

The structure of HC can be described as follows: a large amorphous zone where there are defects and nanonopores and small pseudo-graphite layers in the form of "graphene sheets" [4]. Thanks to this structure, the HC can easily adsorb Na^+. These ions are then intercalated on the graphene layers or they fill the pores present in HC structure.

Ghimbeu et al. [3] suggested that, at low state of charge "SoC", Na^+ can be adsorbed by the pores and defects or they can be inserted by the graphene layers of HC structure. On the other hand, at high SoC, the adsorption of Na^+ on the pores and defects is no longer present. Na^+ are then intercalated into the graphene layers. So the storage mechanism of HC is similar to graphite only at high SoC. This change in Na^+ insertion mechanism can influence the overall performance of a NVPF/HC battery model. Thus, finding a reliable model representing this phenomenon is still a challenge.

According to the Fig. 1a, NVPF/HC batteries generally have a pseudo open circuit voltage "pseudo-OCV" (the voltage of the cell in charge/discharge at low current rate C/50) that consists of three zones:

- **Zone A**: a large plateau at high SoCs (between 50% and 100%), where the surface resistance barely varies as a function of the SoC; Fig. 1b illustrates the galvanostatic electrochemical impedance spectroscopy "GEIS" of the cell at zone A (the green Nyquist plot);
- **Zone B**: a sharp voltage variation around SoC 40-50%. According to Fig. 1b, the cell shows a strong diffusion around this zone. This diffusion is expressed by the presence of a large Warburg impedance on the yellow curve at zone B (the area of the curve where a long 45° slope

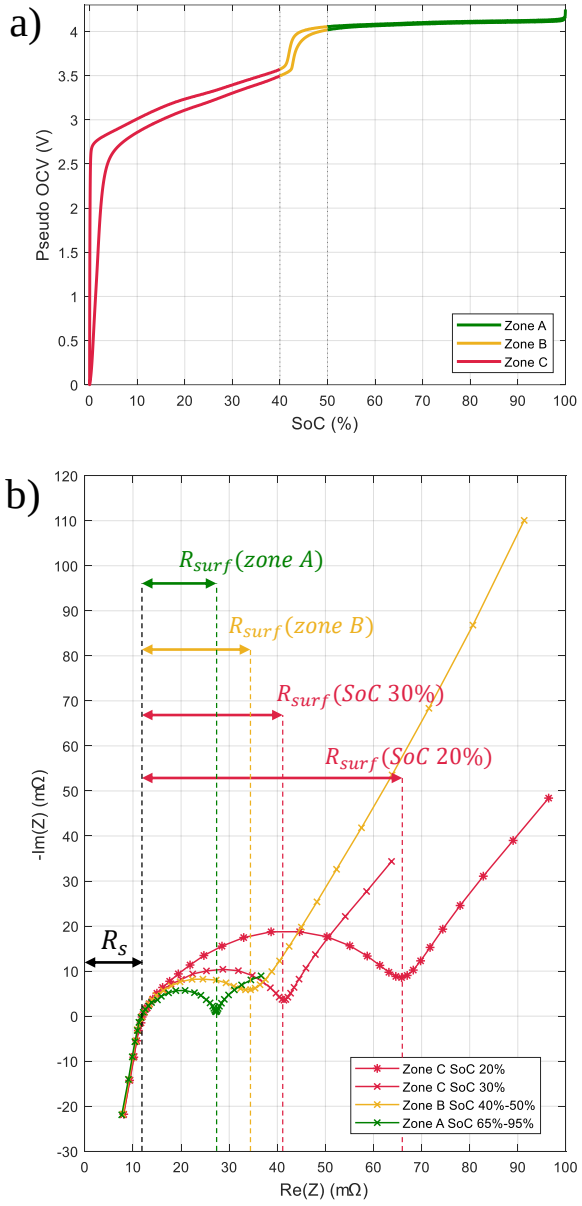

Fig. 1 (a) Pseudo-OCV vs state of charge of NVPF/HC cell at 25 °C (b) GEIS performed on the same cell for each zone at 25 °C

appears after the half circle). So for this study, zone B is avoided due to the presence of the strong diffusion which will not be studied in this paper;

– **Zone C**: a relatively slower voltage variation compared to zone B at remaining SoC range. In zone C, the surface resistance increases strongly with SoC. This is reflected by the big difference in the radii of the red semicircles at SoC 30% and 20% illustrated on Fig. 1b.

Several approaches were proposed to model Li-ion cells. Some were purely physical approaches like the single particle model [5], others were more behavioral like the equivalent circuit model "ECM" [6] and data driven models [7]. ECM model are simpler to integrate in the battery management system "BMS", but this type of model does not always physically present the behavior of the cell.

Damay et al. [8] proposed a model of the so-called "surface resistance" of $LiFePO_4$/graphite cell. This resistance is linked to the voltage drop due to charge transfers and the contribution of solid electrolyte interphase "SEI". The model outputs this resistance as a function of current and temperature, and later separates it into charge transfers resitance and SEI resistance. This could help to better model Na-ion batteries. However, this approach is not treated yet with a hard carbon electrode in which different Na^+ storage mechanisms may occur.

In this preliminary study, we tested the equivalent circuit model ECM and the surface resistance model proposed by Damay et al. on sodium-ion NVPF/HC batteries. This will allow us to know if the surface resistance model works well if the technology of the battery changes. Furthermore, we studied these models at different states of charge (zones A and C) in order to investigate the validity of the surface resistance model for NVPF/HC cells.

In the first part of the paper, the surface resistance model is presented in terms of the Butler-Volmer and Arrhenius equations. In a second part, the experimental protocol related to pulse and GEIS tests is detailed. The choice of states of charge, temperatures and currents is justified in this section. In the third part, the experimental results and the model response are presented for SoC 75% and 25%, followed by an interpretation of the model reliability by varying the SoC of NVPF/HC Cells.

2 Battery model

2.1 Equivalent circuit model

Fig. 2 shows the equivalent circuit model ECM for a Na-ion cell. It has the same structure as Li-ion cell since they have the same electrochemical phenomena. The model is based on an electrical circuit that includes components. These components represent non-linear phenomena. We characterize these components as parameters that depend on current, temperature and SoC:

– $(V^+ - V^-)$ is the cell voltage;
– OCV is the voltage of the cell at equilibrium. It is the open circuit voltage that the cell delivers in the absence of any internal voltage drop;
– R_s is the series resistance which is related to the electronic conduction between the cell and the external circuit. It is an equivalent resistance for any resistive contribution caused by the cell components such as collectors, separators, metallic tabs and cell can;

- R_{surf} and τ_{surf} are respectively the surface resistance and the time constant of the parallel R_{surf}-C_{surf} circuit (τ_{surf} = R_{surf} x C_{surf}). They represent the impedance related to the fast dynamics of the cell. These dynamics include the behavior of the SEI and the charge transfers associated with the double layer effects. Thus, it includes the contributions that takes place between the electrolyte and the surface of the active materials coated on each electrode;
- Z_{diff} is the diffusion impedance related to the slow dynamics. This impedance is linked to the diffusion of Na^+ into the electrolyte and the diffusion of sodium within the active materials in the electrodes. It is presented as the equivalent impedance of n parallel $R_{diff,i}$-$C_{diff,i}$ circuits such that $\tau_{diff,i}$ = $R_{diff,i}$ x $C_{diff,i}$.

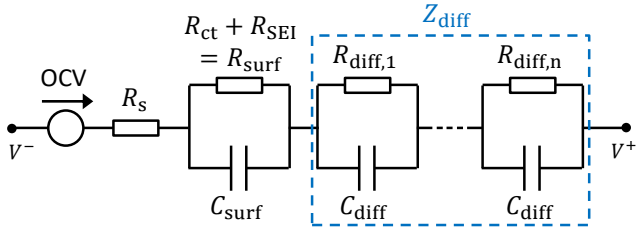

Fig. 2 Equivalent circuit model

2.2 Surface resistance model versus current

In this article, only the surface resistance was considered. This resistance is embedding charge transfers and SEI contributions, which gives:

$$R_{surf} = R_{ct} + R_{SEI} \tag{1}$$

where R_{surf} is the surface resistance, R_{ct} is the charge transfers resistance and R_{SEI} is the SEI resistance.

The behavior of SEI is rather resistive which increases upon cell degradation. We identified the SEI as a resistance since this article presents a model for surface resistances. Soto et al. suggested that the SEI has also a diffusive behavior [9] but it is neglected in this study.

On the other hand, the Butler-Volmer equation was adapted to model the charge transfers. Eq(2) describes the kinetics of electrochemical reactions, related to the cell current I, as a function of the overpotential present at each electrode/electrolyte interface.

$$I = I_0 \cdot \left[\exp\left(\frac{(1-\beta)\cdot F}{RT} \cdot V_{ct} \right) - \exp\left(\frac{-\beta \cdot F}{RT} \cdot V_{ct} \right) \right] \tag{2}$$

where I is the current imposed on the cell (expressed in A), I_0 is the exchange current (in A), β is a dimensionless value that represents the charge transfers coefficient, R is the ideal gas constant (equal to 8.314 $J.K^{-1}.mol^{-1}$), T is the temperature (in K), F is the Faraday constant (equal to 96485.3 $C.mol^{-1}$) and V_{ct} is the charge transfers overpotential (in V).

We assumed that the charge transfers coefficient β is equal to 0.5 [10]. The charge transfers overpotential is defined in eq(3) as the difference between the electrode/electrolyte surface overpotential V_{surf} and the resistive loss caused by the SEI expressed by the resistance R_{SEI}. R_{SEI} is assumed to be independent of the current I.

$$V_{ct} = V_{surf} - I \times R_{SEI} \tag{3}$$

Using eq(2) and eq(3), R_{surf} can be expressed as a function of current through the Butler-Volmer in eq(4):

$$R_{surf}(I) = \frac{V_{surf}}{I} = R_{SEI} + \frac{2RT}{FI} \cdot \text{asinh}\left(\frac{I}{2I_0} \right) \tag{4}$$

According to eq(4), the second term has undetermined value if the current is zero, which means that charge transfers resistance can not be detected at zero current. This problem was solved using Taylor series of the *asinh* function when I is near zero. The charge transfers resistance at 25 °C (298 K) and zero current is then calculated by eq(5):

$$R_{ct,0}(T) = \frac{RT}{F I_0(25\ °C)} \tag{5}$$

2.3 Surface resistance model versus temperature

For the temperature dependence of the surface resistance, the Arrhenius equation allows the rate of a chemical reaction to be described as a function of the temperature. Therefore, Arrhenius law was included in eq(4) in order to model I_0 and R_{SEI} as function of temperature. Hence, eq(6) determines the surface resistance as a function of current and temperature [8]. The first term of eq(6) represents the SEI resistance and the second term represents the charge transfers resistance.

$$R_{surf}(I,T) = R_{SEI}(25\ °C) \exp\left(\frac{E_{a,SEI}}{k_B} \left(\frac{1}{T} - \frac{1}{298} \right) \right) + \frac{2RT}{FI} asinh\left(\frac{I}{2I_0(25\ °C)} \exp\left(\frac{E_{a,I_0}}{k_B} \left(\frac{1}{T} - \frac{1}{298} \right) \right) \right) \tag{6}$$

where k_B is the Boltzmann constant (equal to 8.617 x 10^{-5} $eV.K^{-1}$), $R_{SEI}(25\ °C)$ is the SEI resistance at 25 °C (in Ω), $I_0(25\ °C)$ is the exchange current at 25 °C (in A), and $E_{a,SEI}$ and E_{a,I_0} are respectively the activation energies related to SEI and charge transfers (in eV).

Eq(6) consists of four parameters to be fitted, these parameters are : $R_{SEI}(25\ °C)$, $E_{a,SEI}$, $I_0(25\ °C)$ and E_{a,I_0}.

3 Experimental protocol

For this study, we used a single 18650 NVPF/HC battery provided by Tiamat. It has a maximum voltage of 4.25 V and a minimum voltage that can reach 0V. Its nominal capacity is 700 mAh.

We chose two SoC points to analyze the surface resistance behavior: SoC 75% which corresponds to zone A where Na^+ ions are being inserted in the graphene layers of HC, and SoC 25% which corresponds to zone C where Na^+ are being filled by the pores and defects rather than being inserted. Zones A and C are shown in Fig. 1a.

The battery was tested on three different temperatures: 25 °C, 5 °C and -5 °C, in order to study the cell behavior under usual and extreme conditions.

3.1 Pulse tests

The overall test included charge/discharge steps, i.e. current pulses in opposite directions for a short time. These pulses were performed at several temperatures and SoC points. The test was done in such a way that the SoC point was maintained for every 2 consecutive pulses of opposite directions. These pulse tests were done at different current regimes for 20 seconds. The 20 seconds pulse duration was chosen so that the diffusion process was well fitted without having a deformation of the voltage which is the response of the current pulse [8]. Fig. 3a shows the protocol of the pulse test.

For the temperatures of 25 °C and 5 °C, 12 different current pulses were tested, that is to say 6 pairs of current pulses of opposite directions. These pulses were : (-5C; 5C), (-2C; 2C), (-1C; 1C), (-C/2; C/2), (-C/5; C/5) and (-C/10; C/10). Each pulse was followed by 30 minutes of rest. At -5 °C, the test was slightly modified since it was not possible to charge the tested cell at a high current at a temperature below 0 °C. The negative pulses remained the same, while the positive pulses were set at C/10 with a duration sufficient to recharge the battery with the same amount of charge lost in the previous pulse. For example, a -2C pulse of 20 seconds was compensated by a C/10 pulse of 400 seconds.

The extraction of the ECM model parameters using pulse tests is seen in Fig. 3b.

3.2 GEIS tests

In addition, galvanostatic electrochemical impedance spectroscopy, denoted GEIS tests, at 50mA and then 500 mA amplitudes were applied to the cell for the chosen SoCs and temperatures. The importance of GEIS was to measure the cell impedances near zero current.

GEIS tests at 500 mA amplitude were used to properly measure the series resistance R_s. R_s is the real part of the minimum point of the Nyquist plot before the semicircle. While GEIS at 50 mA were used to determine R_{surf}. R_{surf} is the real part of the semicercle diameter of the Nyquist plot, shown in Fig. 1b. R_{surf} was calculated as the difference between the real of the last point of the semicircle of the Nyquist plot at 50 mA and R_s .

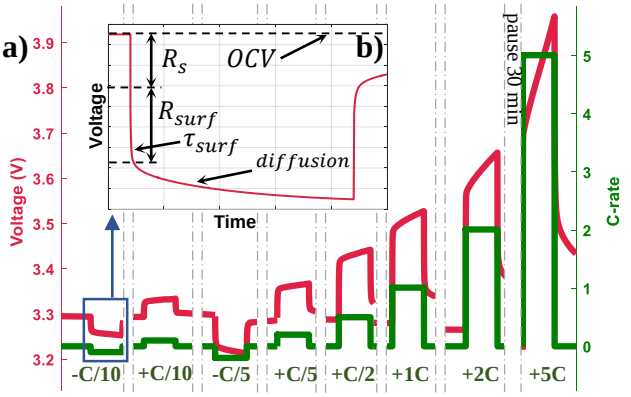

Fig. 3 (a) Current pulses protocol (b) identification of the parameters of the ECM model from the voltage response to a current pulse

4 Results and discussion

4.1 Analysis of the experimental data

GEIS tests showed that the surface resistance varies significantly with SoC and temperature. According to Table 1, the surface resistance increased at low temperatures, which is similar to the surface resistance behavior using $LiFePO_4$/graphite batteries [8]. Moreover, the surface resistance increased remarkably from high SoC (75%) to low SoC (25%). This can be explained by the variation of the Na^+ storage mechanisms in the HC when SoC changes (see introduction).

Table 1 Surface resistance results obtained from GEIS tests

Temperature	[°C]	**25**	**5**	**-5**
R_{surf}(SoC 75%)	[mΩ]	16.1	94.9	311.9
R_{surf}(SoC 25%)	[mΩ]	40.8	471.9	1172.6

For the pluse tests, we chose R_{surf} measurements that result in surface voltage drops of at least 10 mV. For this purpose, we eliminated R_{surf} measurements at 25°C at current regimes of ±C/2 ±C/5 ±C/10 from this study. Because if the magnitude of the voltage drop is smaller than 10 mV, there won't be enough points for fast dynamics fitting. Additionally, we eliminated the pulse test results in the following condition: 5C, 5 °C and SoC 75%. As the cell voltage reached its maximum value of 4.25 V before completing the pulse duration which is 20 seconds.

4.2 Results at high SoC

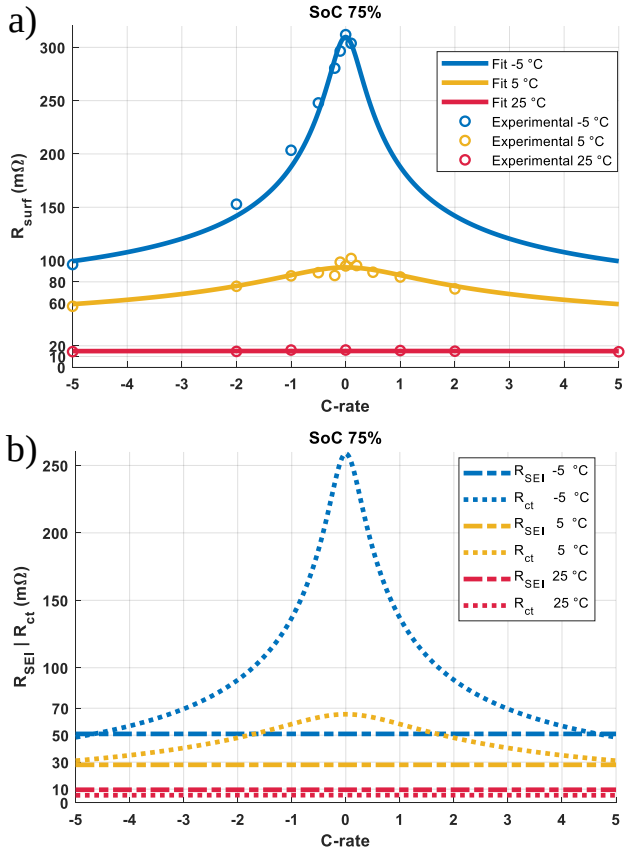

Fig. 4 Results at SoC 75% under different C-rates and temperatures: a) R_{surf} b) seperated R_{ct} and R_{SEI}

Fig. 4a shows the behavior of the resistance as a function of current at SoC 75% and for the three temperatures tested. From Fig. 4a, the estimated surface resistance curve passed through most of the R_{surf} measurements with a root mean squared relative fitting error, denoted RMSRE, equal to 4.2% (see Table 2).

At 25 °C, the surface resistance varied slightly with the current. Meanwhile, at 5 °C and -5 °C, R_{surf} increased at low currents and reached its maximum at a current near 0 mA, then it decreased when increasing the current rate. This study matches with the results already obtained with $LiFePO_4$/ graphite batteries [8].

The SEI and charge transfers resistances are presented in Fig. 4b. At 25 °C, The SEI resistance with a near constant value of 9.6 mΩ was greater than the charge transfers resistance which was close to 5.5 mΩ. At low temperature, the contribution of the charge transfers was greater than that of the SEI because R_{surf} increased significantly at 5 and -5 °C. For example, when charging the cell at 1C at 5 °C, the charge transfers resistance at SoC 75% was 58 mΩ while the SEI resistance was 28 mΩ. At high SoC, the behavior of R_{ct} and R_{SEI} at different current rates and temperatures for the NVPF/HC battery was similar to that of $LiFePO_4$/graphite batteries. Referring to Table 2, the activation energies of SEI was 0.38 eV and that of I_0 was 0.9 eV which are close to the values obtained for $LiFePO_4$/graphite batteries [8].

Table 2 Model parameters

Parameter		SoC 75%	SoC 25%
R_{SEI}(25 °C)	$[m\Omega]$	9.558	9.600
$E_{a,SEI}$	$[eV]$	0.384	0.378
I_0(25 °C)	$[A]$	4.619	0.684
E_{a,I_0}	$[eV]$	0.905	0.874
R_{ct0}(25 °C)	$[m\Omega]$	5.560	37.51
RMSRE	$[\%]$	4.205	20.72

4.3 Results at low SoC

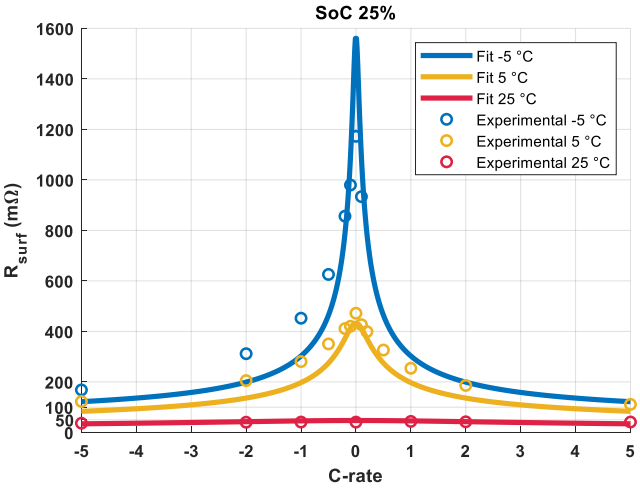

Fig. 5 R_{surf} at SoC 25% under different C-rates and temperatures

Fig. 5 represents the results at SoC 25%. Despite our best efforts, the experimental curve shape was different from the curve shape that the Butler-Volmer equation brought, which means that the proposed surface resistance model can not closely fit the real behavior of the cell.

In order to study the difference between the behaviors at high and low SoC, the fitting results presented on Fig. 5 were obtained by assuming that the SEI parameters, namely R_{SEI} and $E_{a,SEI}$, were the same than those at SoC 75% and then by letting the optimization algorithm fit the charge transfers

parameters. The RMSRE was 20.72%, which can be acceptable for application that does not seek a physical meaning and high accuracy. The activation energy obtained this way for the charge transfers was 0.87 eV, which is still consistent with literature. However, this value should be considered carefully because the model fitting is not accurate and may lack important phenomena. That is why the results of the separation of R_{surf} into R_{ct} and R_{SEI} were not shown.

The problem persisted even if the SEI parameters varies with the SoC with a RSMRE equal to 12.8%. Therefore, the hypothesis that the SEI resistance is invariant to SoC cannot be refuted, nor confirmed.

Given that the proposed R_{surf} model was able to reproduce the cell behavior at SoC 75%, this implies that the cell behavior was strongly changed from SoC 75% to SoC 25%. This was not surprising because the Na^+ storage mechanisms are different for low SoC, as explained in the introduction. The adsorption of Na^+ in the pores and defects of the HC is certainly governed by a different relation between voltage and current, as it was suggested by our fitting results of Fig. 5.

It can be seen that the experimental curve shape was still bell-shaped and centered on zero at low temperatures, which means that the insertion in graphene layers - with a Butler Volmer like behavior - could still be active. The surface resistance model used in this study could maybe be adapted by adding a new term to eq(6) which would represent the adsorption in pores and defects.

5 Conclusion

The surface resistance model with current and temperature dependencies was tested for two different SoCs. The choice of SoCs was based on two different zones of the pseudo-OCV of the NVPF/HC cells where the Na^+ storage mechanisms in hard carbon HC varies.

The model gives good results at high SoC. The relative error is 4.2% and the activation energies are consistent with literature. Classical insertion mechanisms occur in this area and the surface resistance model brings satisfactory results. It is thus possible to characterize the charge transfers and the SEI in these operating regions and get physical insights on these two processes (eg. diagnosis purpose).

However, the model works less well for low SoC with a relative error of 20.72%. The shape of surface resistance measurements and the fit are not the same. Possibly because sodium is not only inserted in HC, but it is also adsorbed via other mechanisms such as adsorption in pores or defects present inside the hard carbon structure. We conclude from this initial study that we can not characterize charge transfers and SEI resistances at low SoC, for sodium-ion batteries with hard carbon in the negative electrode, and that the model should be modified.

This could also imply that, at low SoC, the kinetics of the charge transfer reactions at the HC anode may be slower than those at the NVPF cathode. So the assumption of the charge transfers coefficient β equal to 0.5 may not work at low SoC. Therefore, enhancing the Butler-Volmer equation, by introducing a new term that represent the adsorption of Na^+ in pores and defects and by adjusting β could provide better results.

Another proposal is to separate the charge transfers of the electrodes as two Butler-Volmer equations, one for the cathode and the other for the anode. Moreover, the conclusions of the study concerning the behavior of the HC at low SoC could be applied also to lithium-ion batteries where hard carbon is used as the active material of the negative electrode.

Acknowledgements The authors gratefully acknowledge the financial support from Région Hauts-de-France and Tiamat Energy.

References

1. J.-M. Tarascon, “Na-ion vs. Li-ion Batteries: complementarity rather than competitiveness”, *Joule, Elsevier*, Vol.4 (8), pp.1616-1620, 2020.
2. Q. Abbas, M. Mirzaeian, and M. R. Hunt, “Materials for Sodium-Ion Batteries”, *Encyclopedia of Smart Materials*, pp. 106-114, 2020.
3. C. M. Ghimbeu, J. Górka, V. Simone, L. Simonin, S. Martinet, and C. Vix-Guterl, “Insights on the Na^+ ion storage mechanism in hard carbon: discrimination between the porosity, surface functional groups and defects”, *Nano energy*, Vol. 44, pp. 327-335, 2018.
4. L.-F. Zhao, Z. Hu, W.-H. Lai, Y. Tao, J. Peng, Z.-C. Miao, Y.-X. Wang, S.-L. Chou, H.-K. Liu, and S.-X. Dou, “Hard Carbon Anodes: Fundamental Understanding and Commercial Perspectives for Na-Ion Batteries beyond Li-Ion and K-Ion Counterparts”, *Advanced Energy Materials*, Vol. 11, no. 1, pp. 1-28, 2021.
5. C. Delacourt, “Mathematical Modeling as a Tool for Performance and Aging analysis of Li-ion batteries”, 2014.
6. D. Andre, M. Meiler, K. Steiner, H. Walz, T. Soczka-Guth, and D.U. Sauer, “Characterization of high-power lithium-ion batteries by electrochemical impedance spectroscopy. II: Modelling”, *Journal of Power Sources, Elsevier B.V.*, Vol. 196, pp. 5349-5356, 2011.
7. G. Dong, X. Zhang, C. Zhang, and Z. Chen, “A method for state of energy estimation of lithium-ion batteries based on neural network model”, *Energy*, Vol. 90, pp. 879-888, 2015.
8. N. Damay, K. M. Mbeya, G. Friedrich, and C. Forgez, “Separation of the charge transfers and solid electrolyte interphase contributions to a battery voltage by modeling their non-linearities regarding current and temperature”, *Journal of Power Sources*, Vol. 516 (230617), 2021.
9. F. A. Soto, A. Marzouk, F. El-Mellouhi, and P. B. Balbuena, “Understanding Ionic Diffusion through SEI Components for Lithium-Ion and Sodium-Ion Batteries: Insights from First-Principles Calculations”, *Chemistry of Materials*, Vol. 30, pp. 3315-3322, 2018.
10. M. Farkhondeh, and C. Delacourt, “Mathematical Modeling of Commercial $LiFePO_4$ Electrodes Based on Variable Solid-State Diffusivity”, *Journal of The Electrochemical Society*, Vol. 159 (2), pp. A177-A192, 2011.